Nonlinear effects in small samples of the quasi-one-dimensional conductor TaS₃

D. V. Borodin, S. V. Zaĭtsev-Zotov, and F. Ya. Nad'

Institute of Radio Engineering and Electronics, Academy of Sciences of the USSR

The properties of small TaS₃ samples, with a cross-sectional area $\sim 0.1\,\mu\text{m}^2$ and a minimum length of $5\,\mu\text{m}$, have been studied. The results reveal a region of a negative differential resistance at currents I slightly above a threshold I_T. At $I < I_T$, the differential resistance is a nonlinear function of the current. The threshold field was studied as a function of the length of the sample. The effects observed in small samples may reflect the circumstance that only one or a few of the domains into which the charge density wave is partitioned in TaS₃ can fit in the sample. The phenomena which occur near a current contact have been studied. The experimental results show that the flow of a current up to $50I_T$ on one side of the contact does not alter the properties of the quasi-one-dimensional conductor on the other side, at least at distances greater than $15\,\mu\text{m}$ from the contact. In other words, no nonlocal effects occur in this region on the other side of the contact. In the shortest of these samples (less than $50\,\mu\text{m}$ long) or in the case of narrow contacts (10–$20\,\mu\text{m}$ long), effects stemming from the nonuniform distribution of the electric field near the current contact become important.

1. INTRODUCTION

As the temperature of a quasi-one-dimensional (Q1D) conductor is lowered below a critical value T_p, a Peierls transition occurs, accompanied by the formation of a gap in the energy spectrum and by the condensation of electrons into a charge density wave. Several length scales are used in describing the ground state of a Q1D conductor for $T < T_p$, nonlinear excitations of the conductor, and kinetic effects. The most important of these length scales for an immobile charge density wave ($E < E_T$, where E_T is the threshold field) are the (longitudinal) correlation length ξ, the distance over which phase coherence is preserved in Q1D crystals with impurities, i.e., the Fukuyama-Lee-Rice length[1,2] ξ_{FLR} (this is usually also the length of the average longitudinal dimension of the domains into which the sample may break up[1-3]), and the length L_s, which characterizes the size of the nonlinear excitations of the charge density wave—amplitude and phase solitons.[4,5] After the charge density wave goes into motion, these lengths do not necessarily remain constant. Furthermore, in real crystals it becomes necessary to introduce some new length scales for processes which occur, e.g., near the contacts. One is the length x_0, which corresponds to that distance from the contact over which the phase slippage of the charge density wave occurs,[6] and another is the distance over which the current of the charge density is converted into the current of normal electrons near the contacts, L_0 (Ref. 7). In the Q1D crystals of orthorhombic TaS₃ which we have studied, these lengths are predicted theoretically to be of the following order of magnitude: $\xi \sim 100\,\text{Å}$, $L_s \sim 10^3\,\text{Å}$, and $\xi_{\text{FLR}} \sim 10$–$100\,\mu\text{m}$ (Ref. 8). The values of x_0 and L_0 depend on the electric field: $x_0 \propto (E - E_T)^{-\nu}$, $0.128 \leqslant \nu \leqslant 1$ (Ref. 6), and $L_0 \propto (E - E_T)^{-1/2}$ (Ref. 7). At fields somewhat removed from E_T, where the various transients associated with the onset of motion of the charge density wave have died out, the lenths x_0 and L_0 do not exceed $100\,\mu\text{m}$ in order of magnitude, and they decrease with increasing field.

Until recently, experiments on Q1D conductors such as TaS₃ and NbSe₃ used samples with a length $L \gtrsim 1\,\text{mm}$, which exhibited properties "averaged" over the volume of the sample. Only recently have we seen studies of samples for which the distance between contacts goes down to about $100\,\mu\text{m}$ (Refs. 9–11) The customary way to apply contacts to such samples is to use a conducting paste; this technique imposes a lower limit on the length of the samples. Nevertheless, even these experiments yielded results which demonstrate some specific features of charge density waves at small distances. One such feature is an increase in the threshold field in short TaS₃ samples,[10,11] and another is a blurring of the curves of the Peierls transition.[10] Attempts have been undertaken to study the phenomena which occur near current contacts, at distances $\sim 500\,\mu\text{m}$ (Ref. 12) and $100\,\mu\text{m}$ (Ref. 9).

There was accordingly interest in studying the behavior of charge density waves in short TaS₃ samples, with lengths $L < 100\,\mu\text{m}$, i.e., with $L \sim \xi_{\text{FLR}}, x_0, L_0$. The first experiments in this directions were concerned with the processes responsible for the excitation of narrow-band noise in short TaS₃ samples[13] (with lengths down to $20\,\mu\text{m}$). In the present paper we report the fabrication of stable ohmic contacts separated by distances down to $5\,\mu\text{m}$ by a technique of deposition on thin samples, with a cross-sectional area of $0.1\,\mu\text{m}^2$. We have studied the nonlinear phenomena which occur in these samples and also the phenomena which occur near the contacts.

2. EXPERIMENTAL PROCEDURE

We studied filamentary single crystals of orthorhombic TaS₃. Their cross-sectional areas were 0.1–$0.5\,\mu\text{m}^2$, i.e., two or three orders of magnitude smaller than those of the samples which have customarily been studied. In order to pursue the goal of this study, to determine the properties of charge density waves in samples with small dimensions, it was necessary to develop a technique for applying ohmic contacts of length $l \sim 10\,\mu\text{m}$, separated by distances $L \sim 10\,\mu\text{m}$, to such

0038-5646/86/010184-07$04.00

TABLE I.

Sample	S, μm^2	Sector length L_r, μm	E_T, V/cm ($T = 118$ K)	Sectors with $d^2U/dI^2 > 0$	Symbol used in figures
1	0.09	280, 106, 45, 30	1	280, 106	□
2	0.09	820, 219, 50, 26	1	820	△
3	0.15	118, 82, 24, 24, 21	1	118, 82, 24, 21	○
4	0.30	293, 117, 46, 27, 5	2	–	▽
5	0.38	125, 89, 26, 25, 24	1	–	■
6	0.47	308, 119, 38, 15	1	–	▲
7	0.34	785, 362, 225, 51, 27	0.8	785, 27	●

samples. The existing methods for applying contacts to Q1D materials—the use of conducting pastes and cold indium soldering—can achieve lengths no shorter than $\sim 50\,\mu m$ (Refs. 9–12). The technique which we used made it possible to reduce the minimum contact dimensions and the distances between contacts by yet another order of magnitude. The resulting ohmic contacts have sharp edges and low resistances.

In the fabrication of the contacts, the samples are placed on a glass substrate. The sample is annealed in vacuum at $T = 150$ °C for 30 min and then cooled slowly (over ~ 30 min) in order to clean the surface of the sample. Indium contact stripes are then deposited through special masks. This technique yields ohmic contacts ranging in width from 10 to 30 μm, separated by distances ranging from 5 to 800 μm. The blurring of the boundaries of the resulting contacts is less than 2 μm. The resistance R_c of the contacts at room temperature is determined by the resistance of the indium contact stripes and lies in the range 1–10 Ω. Several contacts are applied to each of the samples, separated by sectors of various lengths. The basic parameters of the test samples and the lengths of the sectors on them are listed in Table I. Samples 1–6 were obtained by splitting one single crystal with a large cross-sectional area, while sample 7 was obtained by splitting another crystal.

Figure 1 shows the sector length L_r, determined from the sector resistances R [using $L_r = (R - R_c)\sigma S$, , where
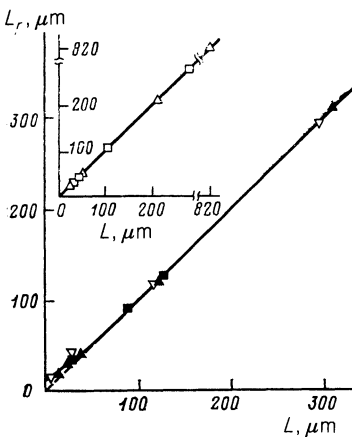

FIG. 1. Comparison of the sector lengths L, determined by an optical method of the TaS_3 samples with the lengths L_r, calculated from the resistance of the sectors at room temperature (samples 4–6). The line rising at an angle of 45° corresponds to the relation $L_r = L$. The inset shows the same behavior, for the samples of the smallest cross-sectional areas (samples 1 and 2).

$\sigma = 3 \cdot 10^3$ S/cm (Ref. 14), and the cross sectional area is determined from the resistance of the longest region, $S = L / \sigma(R - R_c)$] versus the distance L between the edges of the contacts. This distance was measured with an optical microscope. We see that for the thinnest of these samples these lengths are essentially the same. In some cases, however, L_r exceeds L by 5–10 μm for short sectors. As we will show in Section 4 below, this discrepancy stems from the nonuniformity of the electric field near the contacts. In speaking of the "length of a sector" below we will mean the distance L between the edges of the contacts.

We studied the voltage-current characteristics of sectors of various lengths and the behavior of the differential resistance of the sectors as a function of the current through them or through adjacent sectors. All the measurements were carried out at a given current. The low resistance of the contacts made it possible to measure the voltage-current characteristics of the sectors by a two-contact method. The output resistances of the dc and ac power supplies were at least 1 GΩ and 0.2 GΩ, respectively; the modulation frequency was 22 Hz. The amplitude of the current modulation was $\tilde{I} \sim 10^{-2} I_T \sim 10^{-9}$ A (I_T is the threshold current). The high resistances of the test samples (10^4–10^6 Ω at $T = 120$ K) and—in several cases—the low values of the measured voltages ($\sim 10^{-6}$ V) required careful shielding of the measurement apparatus against noise and stray pickup. The low-frequency noise level at the test samples, at currents below the threshold, was on the order of the Johnson noise. The temperature was regulated with 40 mK at $T = 120$ K, keeping the error in the resistance measurements at $\sim 0.1\%$.

3. EXPERIMENTAL RESULTS

Over the range 240–100 K, the temperature dependence $\sigma(T)$ of our TaS_3 samples with small cross-sectional areas has the shape typical of pure samples.[15] At $T \sim T_p$, however, the shape of the $\sigma(T)$ curve depends on the length of the sectors under study.[10] For regions less than 30 μm long we observe a broadening of the $d \ln \sigma(T)/d(1/T)$ curve near T_p. This broadening is particularly noticeable for a very short region, with $L = 5 \mu m$. We also see a slight shift of the minimum of this curve, corresponding to the point $T = T_p$, toward higher temperatures. For sample 1, for example, this minimum shifts from 217 K ($L = 280$ μm) to 220 K ($L = 30$ μm). In a study of samples with a cross-sectional area 10^2–10^3 times those in the present experiments, Mihály et al.[10] observed a similar broadening of the $\sigma(T)$ curve near T_p for samples with a length as great as 300 μm. The activa-
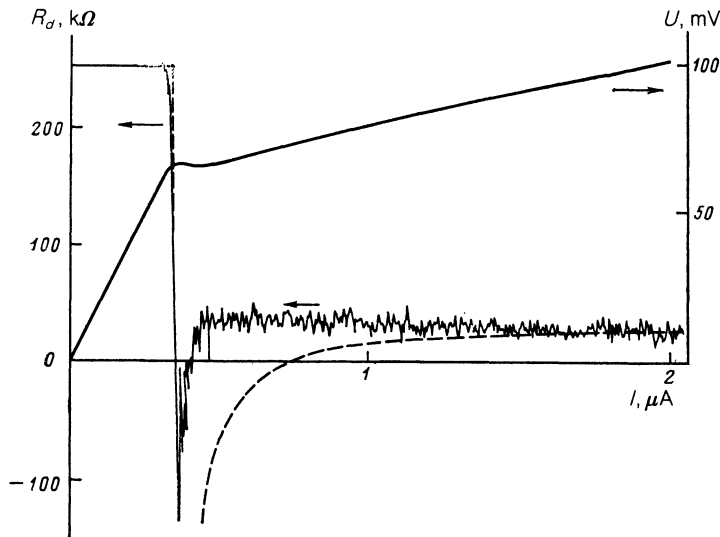
FIG. 2. Voltage-current characteristic and current dependence of the differential resistance for a sector $L = 785$ μm long of sample 7 ($T = 137$ K). The curves were recorded as the current was reduced. The dashed line shows the functional dependence R_d (I) calculated in accordance with Ref. 20.

tion region of the $\sigma(T)$ dependence at $T < 200$ K does not charge with decreasing L, within the experimental errors.

The shape of the voltage-current characteristics of our TaS$_3$ samples of small cross-sectional area also depends on the length of the sector. We found that the characteristics for sectors more than 100 μm long have a nonstandard shape. In Fig. 2, which shows a voltage-current characteristic at $T = 137$ K, we see, above the threshold current, an abrupt change in slope and a region of a negative differential resistance, followed by an approximately linear region of $U(I)$ (for $I < 3I_T$). Also shown in Fig. 2 is the current dependence of the differential resistance $R_d = dU/dI$ of the same sample. Near $I = I_T$, R_d decreases sharply, going negative, and then goes onto a plateau; here we see the low-frequency noise generation, which sets in at $I > I_T$. The voltage-current characteristics and the R_d (I) dependence retain this shape, regardless of whether the current is raised or lowered and regardless of the polarity of the current. This shape of the voltage-current characteristic, consisting in a sense of two linear regions [$I < (3-5)I_T$], is retained over the entire temperature range studied, 100–160 K. As the temperature is lowered below 120 K, on the other hand, the region with a negative differential resistance becomes progressively more difficult to make out and disappears, while the characteristic retains a transition region: a region with a positive curvature, $d^2U/dI^2 > 0$, which persists down to $T = 100$ K. A similar blurring of the region of a negative differential resistance is found at $T > 150$ K. The region of negative differential resistance turns out to be sensitive to thermal cycling. After a few cycles of cooling to 100 K and heating to 300 K, the negative differential resistance usually disappears, but the voltage-current characteristic retains the shape described above.

As the length of the sector of the sample decreases to $L < 100$ μm, the general shape of the voltage-current characteristic also begins to change. Figure 3 shows a series of normalized characteristics at $T = 118$ K for sectors of various lengths on a common sample. While the shape of the characteristics changes only slightly with the length of the sector at $L > 100$ μm, at $L < 50$ μm we see a blurring of the sharp

transition at $I \approx I_T$ and also a decreease in the ratio of the slopes of the regions at $I < I_T$ and $I > I_T$. In other words, the nonlinearity of the voltage-current chracteristics becomes less pronounced. In the samples (1–3) with the smallest cross-sectional area, the slow change at $I \approx I_T$ on the characteristic is retained even for the sectors of lengths $L \sim 20$–30 μm (see the inset in Fig. 3).

Figure 4 shows results found on R_d (I) for sectors of various lengths (sample 7) versus the current at $T = 119$ K. We see directly from these curves that the nonlinearity of the voltage-current characteristic decreases with decreasing length of the sector; this decrease in nonlinearity is seen as a decrease in the ratio of R_d ($I = 0$) to R_d ($I > I_T$), but there is still a tendency toward the appearance of a minimum in R_d at $I \gtrsim I_T$ (a sector with $L = 27$ μm). In the long TaS$_3$ samples which we studied, as can be seen from the example of sample 7 (Fig. 2, $L = 785$ μm), R_d remains constant up to $I = I_T$, while in the short samples, beginning at $L \sim 100$ μm, we see slight changes (up to 10%) at R_d at currents below the threshsold. These changes are reproducible when the measurements are repeated ($I < I_T$). When the direction in which the curve is measured is reversed, and we go beyond I_T, we frequently see hysteresis in these oscillations (see the
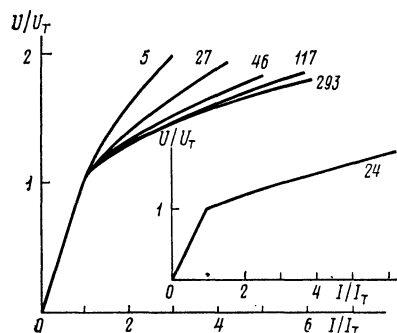

FIG. 3. Series of normalized voltage-current characteristics of sectors of various lengths (sample 4). The inset shows the voltage-current characteristic of a sector of a sample with a small cross-sectional area (Sample 3). The curves are labeled with the length of the sector in microns ($T = 118$ K).
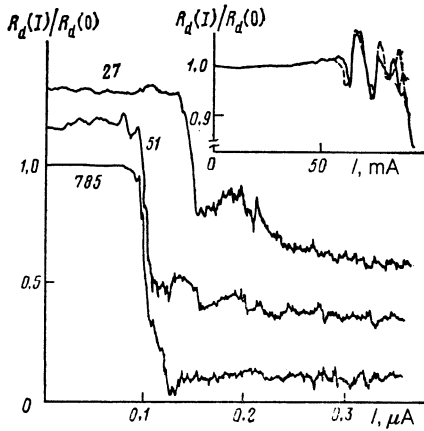
FIG. 4. The normalized differential resistance $R_d(I)/R_d(0)$ versus the current for sectors of various lengths (sample 7). The curves are labeled with the length of the sector, in microns. The curves for the sectors 51 and 27 μm long are displaced vertically by 0.15 and 0.30, respectively. The inset shows a fragment of the corresponding curve for sample 3 (for a sector 118 μm long), recorded as the current was increased (solid line) and decreased (dashed line) ($T = 118$ K).

inset in Fig. 4). Noise generation is observed here only after the sharp decrease in R_d (Fig. 4).

According to the results of Refs. 10 and 11, as the sector length is reduced to $L < 100\,\mu$m we could expect the threshold field E_T to decrease substantially. Figure 5 shows some typical results on the threshold voltage U_T as a function of the length of the sector for two of the samples. On the whole, U_T decreases in proportion to the length of the sector. An extrapolation of $U_T(L)$ to $L = 0$, however, yields a nonzero value: $U_T(0) = 0.5$–1 mV. Accordingly, the field $E_T = U_T/L$ increases 10–30% as L is reduced from 300–800 to 30 μm (see the inset in Fig. 5). This increase, however, is not as pronounced as might be expected on the basis of the data of Refs. 10 and 11, where samples with lower values of E_t ($E_t \sim 0.5$ V/cm at $L \sim 700\,\mu$m) and significantly larger cross-sectional areas ($S = 50$–70 μm^2) were studied. The temperature dependence of the threshold field for the sectors of various lengths is basically the same for our samples at $100 \lesssim T \lesssim 180$ K and similar to the results reported in Refs. 10 and 15.

Since the results discussed above demonstrated changes in the behavior $\sigma(T)$, $U(I)$, and $R_d(I)$ with decreasing sector length, we took up a study of the processes occurring in the regions near the contacts, which might be important in
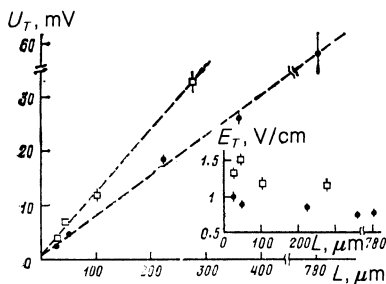

FIG. 5. Threshold voltage versus the length (samples 1 and 7). The inset shows the dependence of the threshold field on the length for the same samples ($T = 118$ K).
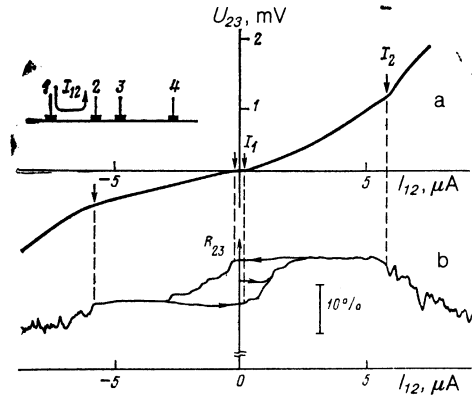

FIG. 6. The voltage U_{23} and the resistance R_{23} of sector 2–3 versus the current I_{12} (sample 5, $T = 118$ K). The length of sector 2–3 is 25 μm, and the length of contact 3 is 16 μm. The arrangement of contacts is shown in the inset. The arrow shows the positive current direction ($I_{12} > 0$).

determining the properties of short sectors. For this study we used a sample with several contacts, separated by various distances (see the inset of Fig. 6). We measured the voltage U_{23} and the sector resistance R_{23} as functions of the current I_{12} in an adjacent sector (Refs. 9 and 12). In the case of wide contact stripes ($l \gtrsim 30\,\mu$m), in which the total contact resistance is determined primarily by the ohmic resistance of these conducting films ($R_c \sim 1$–10 Ω), the $U_{23}(I_{12})$ dependence is linear (the error here is 10%) up to $I_{12} = 50I_T$ [$U_{23}(50I_T) \leqslant 100\,\mu$V]. In the case of narrower stripes, of width $l \sim 10\,\mu$m, structural features appear on the $U_{23}I(I_{12})$ curve (Fig. 6a). These are bends near currents I_1 and I_2, where I_1 is equal to the threshold current I_T of sector 1–2. In the region $|I_{12}| < I_1$ the $U_{23}(I_{12})$ dependence is linear, while near I_2 we sometimes see jumps in the voltage and a hysteresis. When the polarity of the current is switched, all these structural features are basically preserved, but the curve of $U_{23}(I_{12})$ at $|I_{12}| > I_1$ is not perfectly symmetric in the current: $U_{23}(I_{12}) > |U_{23}(-I_{12})|$. As the temperature is lowered, this asymmetry of the $U_{23}(I_{12})$ curve becomes more pronounced. The voltage U_{23} depends on the size of the contact, decreasing with increasing length of the contact. For contacts with approximately equal lengths, U_{23} depends on the cross-sectional area of the sample. For a given ratio I_{12}/I_T, the voltage U_{23} is higher for the samples of larger cross-sectional area.

Figure 6b shows the typical behavior of the sector resistance R_{23}, measured at a low alternating current $\tilde{I}_{23} \lessdot I_T$, flowing in the same sector, as a function of the current I_{12} in the adjacent sector. Here we typically see hysteresis at $|I_{12}| < I_2$, with the beginning of a transition from one branch to the other at I_1 and $-I_1$; at $|I_{12}| > I_2$ we see a slight decrease in R_{23} ($\sim 10\%$) and an increase in the low-frequency noise. The direction along which the hysteresis loop is traced out is the same for all the samples studied. The hysteresis which we observe is apparently due to the presence of metastable[16,17] or bistable[18] states in TaS$_3$ near the contact. Further research is required to determine the physical nature of this hysteresis and also the nature of the asymmetry of the $U_{23}I(I_{12})$ curves.

The resistance (which may be nonlinear) of current

contact 2 contributes to some extent to the value of $U_{23}(I_{12})$ measured in a three-contact arrangement. For more reliable measurements of the effects beyond a current contact we carried out measurements with a four-contact arrangement (see the inset in Fig. 6), separating the functions of the current contact (2) and the potential contact (3). We found that at distances $L_{23} = 24\,\mu m$ between the current contact and the potential contact (sample 3; contacts of length $l = 11\,\mu m$) the value of U_{34} at $I_{12} = 50I_T$ is less than the resolution of these measurements, $\sim 1\,\mu V$, while at $L_{23} = 15\,\mu m$ (sample 6; contacts of lengths $l = 10$ and $14\,\mu m$ we find $U_{34} \leqslant 2\,\mu V$. The change in the resistance of sector 3-4 is $\Delta R_{34}/R_{34} \leqslant 0.1\%$ at $|I_{12}| \leqslant 50I_T$. Consequently, no "nonlocal" effects ("nonlocal" with respect to the region in which the current I_{12} flows) were observed in a region of the sample $15\,\mu m$ from the current-flow region.

4. DISCUSSION OF RESULTS

Most of the previous studies of the properties of Q1D materials such as TaS_3 and $NbSe_3$ have used samples whose volumes have contained 10^3–10^4 domains,[8] i.e., regions along which the phase of the charge density wave may change by $\sim 2\pi$ as a result of interactions with impurities. This phase change occurs over a distance (along the axis of highest conductivity) equal to the Fukuyama-Lee-Rice length ξ_{FLR}. In the present experiments we have studied TaS_3 samples with small transverse and longitudinal dimensions, with volumes three to five orders of magnitude smaller than those of the samples in the previous studies. We might therefore expect that in the present experiments we have attained or at least approached the characteristic length ξ_{FLR} for phase coherence and, in the narrowest samples, situations in which the volume of the sample contains only one or a few domains.

The increase in T_p with decreasing sample volume which we observe in the $\sigma(T)$ dependence may arise because three-dimensional ordering processes at $T = T_p$ take place more easily in samples with only a few domains. The transition is somewhat blurred; this blurring occurs in samples far shorter ($\sim 10\,\mu m$) than in Ref. 10, where a study was made of samples with a large cross-sectional area. The apparent reason for this blurring is a manifestation at these sample lengths of field nonuniformities near the contacts (this question is discussed in more detail below).

A charge density wave in a sample containing only a single domain is, in a sense, weakly coupled with the impurities in it, and at $I > I_T$ the charge density wave can move as a "rigid" unit. In this case we can use the phenomenological[19,20] and microscopic[3,4] theories for a rigid charge density wave. It follows, in particular, from these theories that the voltage-current characteristic of a single-domain sample should have a sharp bend near the threshold current I_T and a region of positive curvature, with $d^2U/dI^2 > 0$. This is precisely the shape of the voltage-current characteristic which we observe for many of the narrowest samples which we studied (see Table I and the inset in Fig. 3), while in the larger TaS_3 samples which have usually been studied the region of the bend in the voltage-current characteristic near

I_T is blurred.[10] Furthermore, it follows from the phenomenological model of Ref. 20 that when the current is specified we should observe a region with a negative differential resistance on the voltage-current characteristic of a single-domain sample. Shown for comparison in Fig. 2 is the theoretical prediction of Ref. 20 (the dashed line). We see that there is a qualitative agreement with experiment. We could apparently expect better agreement by using the microscopic theory of Ref. 3, but the $R_d(I)$ dependence was not taken up in Ref. 3.

Further evidence for the possibility that we are dealing with a situation with few domains in these samples comes from the oscillations which we found on the $R_d(I)$ curve at currents below the threshold (Fig. 4). These oscillations can be attributed to changes in the structure of individual regions of a charge density wave (or of individual domains), which occur at currents below the threshold, where the charge density wave as a whole is not yet moving.[21] In principle, the value of R_d, which at $I < I_T$ is determined by the free electrons which are carrying the current, could change slightly because the way these electrons scatters changes when the configuration of the pinned charge density wave changes, in particular, through the creation of static solitons by an electric field in this wave.[22] These oscillations are visible in the smaller samples; in the long and thick samples, they may be effectively averaged out because of a weak correlation in a large number of domains. However, further research is required to verify these suggestions.

The voltage-current characteristics for sectors of a given sample change only slightly as the sector length L is varied over the range 300–100 μm. As the sector length is reduced further, we would expect to approach a clear single-domain pattern. The experiments show, however, that in most samples the nonlinearity of the voltage-current characteristic decreases with decreasing L (Fig. 3), and only in the samples with the smallest cross-sectional area ($S \sim 0.1\,\mu m^2$) does a voltage-current characteristic with a clearly defined slope change persist to $L \sim 20$–$30\,\mu m$. In those samples in which we observe a region of negative differential resistance, this region becomes blurred and disappears as the sector length is reduced ($L \leqslant 100\,\mu m$). The threshold field begins to increase at approximately the same lengths (Fig. 5). The most natural suggestion is that the contact regions are beginning to have an important effect on the properties of the short samples. Near the contacts, the current of the charge density wave changes into a current normal-carrier, and phase-slippage centers of the charge density wave appear.[6,7,23] In principle, the length scales for these processes may not be very small; if they are not, there could be changes in the shape of the voltage-current characteristics of short samples and an increase in the threshold field. Furthermore, the use of lateral contacts to a highly anisotropic sample in the overwhelming majority of the studies (including the present study) means that there is a region with a nonuniform electric field near the contacts. We will show below that these regions play a very imporant role in short samples. We will thereby show that it is the properties of the contact which are responsible for many of the phenomena which are observed beyond a contact.
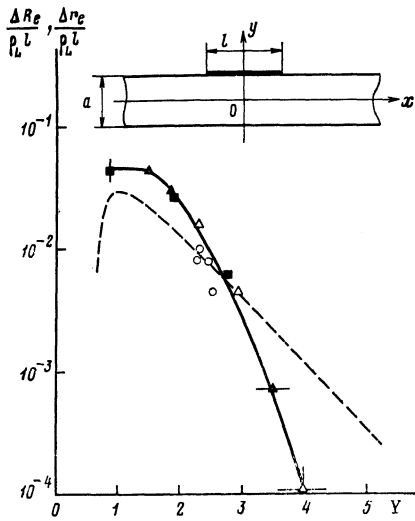
FIG. 7. The quantity $\Delta R_e/\rho_L l$ versus the dimensionless contact length Y (samples 3–6, $T = 118$ K). Dashed line—theoretical behavior of $\Delta r_e/\rho_L l$ according to (2) as the anisotropy (A) of the conductivity is increased by a factor of four (see the text proper); inset—schematic diagram of the contact.

As a model of the contact we consider a metal electrode of length l deposited on the upper face of a Q1D conductor of rectangular cross section $a \times b$ (see the inset in Fig. 7). We place the origin of coordinates under the middle of the contact, at the center of the sample. The x axis is directed along the axis of the sample, and the y axis is perpendicular to the plane of the figure. In an anisotropic Q1D conductor we would have $\sigma_{xx} = A\sigma_{yy} = A\sigma_{zz} = \sigma$; $\sigma_{ij} = 0$ $(i \neq j)$. We assume that the second contact is at $x = +\infty$ (Ref. 24), we can solve the problem of the spatial distribution of the potential in the volume of the conductor by conformal mapping. We find the following expression for the potential profile along the upper face of the sample:

$$U(x) = -\frac{aA^{1/2}E}{\pi}\,\mathrm{arcch}\left|\frac{\mathrm{ch}\,(\pi l/2aA^{1/2}) - \exp(\pi x/aA^{1/2})}{\mathrm{sh}\,(\pi l/2aA^{1/2})}\right|,$$

$$|x| \geqslant l/2,$$

where $E = -\lim_{x\to\infty} dU/dx$ is the electric field far from the contact. A quantity of importance for comparison with experiment is

$$r_i = \lim_{x\to\infty}\frac{U(x) + (x - l/2)E}{I}$$

$$= \frac{2\rho_L aA^{1/2}}{\pi}\ln[2/(1-\exp(-4Y))], \qquad (1)$$

where $Y = \pi l/4aA^{1/2}$ is the dimensionless length of the contact, and $\rho_L = (\sigma ab)^{-1}$ is the resistance per unit length of the sample. The quantity r_i is the increment in the resistance of the sample which results from the nonuniformity of the field distribution ahead of the contact; i.e., the total resistance of a sector of length L is written $R = \rho_L L + 2r_i$. The r_i contribution is most important in short samples, with $\rho_L L \sim 2r_i$, i.e., $L \sim aA^{1/2} \sim 5$–$10\,\mu$m (Fig. 1). The presence of this contribution and its dependence on ρ_L and A can obviously be explained in terms of a decrease in the nonlin-

earity of the voltage-current characteristic as the samples become shorter (Figs. 3 and 4). The anomaly in the temperature dependence of the anisotropy of the conductivity near T_p (Ref. 25) explains the difference between the behavior $\sigma(T)$ for short TaS$_3$ samples and the corresponding behavior for long TaS$_3$ samples which was observed in Ref. 10 and in the present study.

We turn now to the behavior of $U_T(L)$ (Fig. 5). What contribution is made to this quantity by effects stemming from the nonuniformity of the electric field ahead of the current contacts? At $I = I_T$ we have

$$U_T = (L\rho_L + 2r_i)I_T ,$$

and the correction, $2r_i I_T \approx E_T aA^{1/2} = 0.5$–1 mV is found to be comparable in magnitude to $U_T(0)$. Accordingly, a voltage drop across r_i can make a significant contribution to the nonzero value of $U_T(0)$ which is found experimentally (Fig. 5). This effect apparently could also have made an important contribution to the decrease in E_T observed in Ref. 10 as the length of the samples was reduced to $100\,\mu$m. Nevertheless, we note that for the samples which we studied the threshold current for short sectors $(L = 10$–$12\,\mu$m) is 10–50% above that for long sectors (Fig. 4), possibly indicating a change in the properties of the region near the contact because of current conversion processes[6,7] there and because the phase of the charge density wave slips.[6,7,23] The pronounced nonuniformity of the electric field over the entire length and cross section of a short sample thus poses severe difficulties for measurements and analysis of the motion of a charge density wave, the shape of the voltage-current characteristic, and the magnitude of the threshold field. The experimental way to overcome these difficulties is to to use materials with less anisotropy, samples with a small cross-sectional area, and ultimately, to put end contacts on the samples.

We turn now to the processes which occur beyond the current contact. A quantity of importance to an understanding of these processes is

$$r_e = \lim_{x\to-\infty}\frac{U(x)}{I} = \frac{\rho_L l}{4Y}\ln\mathrm{cth}\,Y. \qquad (2)$$

In the case of a narrow contact $(Y \ll 1)r_e = r_i = -(\rho_L aA^{1/2}/\pi)\ln(1/Y)$ is a two-dimensional analog of the spreading resistance, which is familiar in the case of point contacts and which is manifested as a resistance of the contact. For an extended contact, however, there is no unique quantity which plays the role of a spreading resistance to which we can reduce the nonuniformity of the electric field on both the left and right of the contact. Under the condition $Y \gg 1$, we find from (1) and (2)

$$r_i = (2\ln 2/\pi)\rho_L aA^{1/2}, \quad r_e = (2/\pi)\rho_L aA^{1/2}\exp(-\pi l/2aA^{1/2}),$$

i.e., $r_i \gg r_e$. The quantity r_e is an exponential function of the anisotropy of the conductivity, A, which in turn changes at $I > I_T$.

Let us use these results to analyze the behavior shown in Fig. 6 for sample 5.

1. $I_{12} < I_1$. In this region, the function $U_{23}(I_{12})$ is linear and is determined by the sum of r_e and the resistance of the indium contact stripe, r_s: $U_{23} = (r_e + r_s)I_{12}$.

2. $I_1 < I_{12} < I_2$. In this region, the function $U_{23}(I_{12})$ becomes nonlinear. However, the resistance of sector 2–3 remains the same if we are on the corresponding branch of the hysteresis loop (Fig. 6). It follows that the properties of sector 2–3 remain the same, and the nonlinear increase in the quantity

$$U_{23}(I_{12}) = [r_e(I_{12}) + r_s] I_{12}$$

stems from the nonlinear increase in r_e, which in turn is caused by the change in the anisotropy of the conductivity in sector 1–2 near contact 2 [see (2)].

3. $I_{12} > I_2$. The resistance of sector 2–3 decreases, and the low-frequency noise in it increases. This behavior may arise because the boundary between the moving and fixed parts of the charge density wave, under contact 2, approaches sector 2–3. Since we have $R_{23} = L_{23}\rho_L + r_{i2} + r_{i3}$ (r_{i2} and r_{i3} are the resistances r_i of contacts 2 and 3 for the small alternating current $\tilde{I}_{23}$ which is used to measure R_{23}), as this boundary approaches sector 2–3 there should be a change primarily in the contribution to R_{23} from R_{i2} because of the change in the conductivity and the anisotropy under contact 2 [see (1)]. It follows from the experimental results (Fig. 6) that even at $I_{12} = 50I_t$ the quantity ΔR_{23} is small: $\Delta R_{23} \approx 0.1R_{23}$. This result is equivalent to a shift of the boundary between the moving and the fixed parts of the charge density wave over a distance $\Delta L \sim 0.1L_{23} \sim 2$–$3\,\mu$m; here $\Delta L\rho_L \sim r_{i2}$. The current I_{12} thus changes the properties of only a small region near contact 2, no larger than the distance to which the static, nonuniform electic field from sector 1–2 penetrates beyond contact 2. The magnitude of this effect depends on the particular geometry of the contact, i.e., on Y—not exclusively on its length l, as might be expected if nonlocal effects dominated.[12] For a thin sample with a shorter contact (sample 3, $l = 11\,\mu$m), for example, we would expect nonlocal effects to be very influential. What we find, in contrast, is that ΔR_{23} is nearly an order of magnitude smaller than in sample 5 (Fig. 6): $\Delta R_{23} = 0.01R_{23}$, with $\Delta L \sim 0.2\,\mu$m ($I_{12} = 50I_T$).

The absence of nonlocal effects over distances $\sim 10\,\mu$m is confirmed by the following result. From (2) we find that the quantity

$$r_e/\rho_L l = (4Y)^{-1} \ln \operatorname{cth} Y$$

depends on the dimensionless contact length Y. If we assume that at some $I' > I_T$ the conductivity and anisotropy change identically over the entire sample, not exclusively in sector 1–2, then we an also use expression (2) for r_e. The dashed line in Fig. 7 shows the normalized different $(r_e' - r_e)/\rho_L l = \Delta r_e/\rho_L l$ as a function of Y, where r_e' corresponds to $A' = 4A$ and $\rho_L' = \rho_L/4$. Also shown in this figure are values found experimentally for the quantity

$$\Delta R_e/\rho_L l = [R_e(50\,I_T) - R_e(0)]/\rho_L l,$$

where $R_e = U_{23}/I_{12}$, versus the dimensionless contact length Y. The values of Y for each of the contacts were determined from (2) with the experimental values of l, ρ_L, and r_e ($|I_{12}| < I_T$). We see that the experimental points found for the different contacts and for the different samples conform to one curve, common to all the samples (the solid line in Fig. 7), similar to the curve which follows from the simple model described above. Consequently, to predict the properties of a contact at $I_{12} > I_T$ it is sufficient to know its dimensionless length at $I_{12} < I_T$ (and not l). We do not need to appeal to more complex effects[12] in order to explain behavior like that in Fig. 6.

In summary, the results of these measurements of the functions $U_{23}(I_{12})$ and $R_{23}(I_{12})$ can be explained both qualitatively and quantitatively in terms of effects which stem from the nonuniformity of the electric field near a contact and from the change in this nonuniformity in fields above a threshold level. Important in this connection are the results of measurements by the four-contact method (see the inset in Fig. 6). The absence of any significant voltage in sector 3–4 during the passage of a current in sector 1–2, 15 μm away, is direct experimental confirmation that no nonlocal effects of any sort occur at distances greater than 15 μm from the contact. The nonlocal effects observed in TaS$_3$ in Ref. 12 with a scale length $\sim 50\,\mu$m are not seen in the present experiments.

We wish to thank A. F. Volkov for a discussion and Y. A. Savitskaya for furnishing the samples.

[1] H. Fukuyama and P. A. Lee, Phys. Rev. **B17**, 535 (1978).

[2] P. A. Lee and T. M. Rice, Phys. Rev. **B19**, 3970 (1979).

[3] R. A. Klemm, M. O. Robbins, and J. R. Schrieffer, in: Proceedings of the International Conference on Charge Density Waves in Solids, Budapest, Hungary, 1984 (ed. Hutiray and J. Solyom), Vol. 217, Lecture Notes in Physics, Springer-Verlag, Berlin, 1985, p.178.

[4] S. N. Artemenko and A. F. Volkov, Zh. Eksp. Teor. Fiz. **80**, 2018 (1981) [Sov. Phys. JETP **53**, 1050 (1981); **81**, 1872 (1981) [**54**, 992 (1981)]].

[5] S. A. Brazovskiĭ, Zh. Eksp. Teor. Fiz. **78**, 677 (1980) [Sov. Phys. JETP **51**, 341 (1980)].

[6] L. P. Gor'kov, Zh. Eksp. Teor. Fiz. **86**, 1818 (1984) [Sov. Phys. JETP **59**, 1057 (1984)].

[7] S. N. Artemenko and A. F. Volkov, Pis'ma Zh. Eksp. Teor. Fiz. **40**, 74 (1984) [JETP Lett. **40**, 811 (1984)].

[8] L. Mihály and G. Grüner, Solid State Commun. **50**, 805 (1984).

[9] J. C. Gill, Solid State Commun. **44**, 1041 (1982).

[10] G. Mihály, Gy. Hutiray, and L. Mihály, Phys. Rev. **B28**, 4894 (1983).

[11] G. Mihály, Gy. Hutiray, and L. Mihály, Solid State Commun. **48**, 203 (1983).

[12] Yu. I. Latyshev, Ya. S. Savitskaya, and V. P. Fralov, Pis'ma Zh. Eksp. Teor. Fiz. **40**, 72 (1984) [JETP Lett. **40**, 807 (1984)].

[13] D. V. Borodin, S. V. Zaĭtsev-Zotov, and F. Ya. Nad', Pis'ma Zh. Eksp. Teor. Fiz. **41**, 340 (1985) [JETP Lett. **41**, 416 (1985)].

[14] T. Sambongi, K. Tsutsumi, Y. Shiozaki, et al., Solid State Commun. **22**, 729 (1977).

[15] Z. Z. Wang, H. Salva, P. Monceau, et al., J. Phys. (Paris) **44**, L311 (1983).

[16] A. W. Higgs and J. C. Gill, Solid State Commun. **47**, 737 (1983).

[17] G. Mihály and L. Mihály, Solid State Commun. **48**, 449 (1983).

[18] N. P. Ong, D. D. Duggan, C. B. Kalem, T. W. Jing, and P. A. Lee, in: Proceedings of the International Conference on Charge Density Waves in Solids, Budapest, Hungary, 1984 (ed. Hutiray and J. Solyom). Sol. 217, Lecture Notes in Physics, Springer-Verlag, Berlin, 1985, p. 387.

[19] G. Grüner, A. Zawadowski, and P. M. Chaikin, Phys. Rev. Lett. **46**, 511 (1981).

[20] R. Monceau, J. Richard, and M. Renard, Phys. Rev. **B25**, 931 (1982).

[21] R. B. Littlewood, in: Proceedings of the International Conference on Charge Density Waves in Solids, Budapest, Hungary, 1984 (ed. Hutiray and J. Solyom). Vol. 217, Lectures Notes in Physics, Springer-Verlag, Berlin, 1985, p. 369.

[22] K. Maki, Phys. Rev. Lett. **39**, 46 (1977).

[23] N. P. Ong, G. Verma, and K. Maki, Phys. Rev. Lett. **52**, 663 (1984).

[24] L. Van der Pau, Philips Res. Rep. **16**, 187 (1961).

[25] M. Ido, K. Kawabata, and T. Sambongi, Mol. Cryst. Liq. Cryst. **81**, 91 (1982).

190   Sov. Phys. JETP **63** (1), January 1986

Borodin *et al.*   190